



Vertical distribution of mercury, CO, ozone, and aerosol scattering coefficient in the Pacific Northwest during the spring 2006 INTEX-B campaign

P. C. Swartzendruber,^{1,2} D. Chand,^{1,2} D. A. Jaffe,^{1,2} J. Smith,² D. Reidmiller,^{1,2} L. Gratz,³ J. Keeler,³ S. Strode,¹ L. Jaeglé,¹ and R. Talbot⁴

Received 7 November 2007; revised 31 January 2008; accepted 14 February 2008; published 29 May 2008.

[1] In the spring of 2006, we measured the vertical distribution of gaseous elemental mercury (GEM), CO, ozone, and aerosol scattering coefficient in the Pacific Northwest concurrent with NASA's INTEX-B campaign. Seven profiles from the surface to 6 km were conducted from 12 April to 8 May along with one flight in the Seattle-Tacoma boundary layer. Ozone had a bimodal distribution with the lower mode occurring primarily in the mixed layer and the higher mode occurring in the free troposphere. In the free troposphere, the mixing ratios ($1 - \sigma$) of GEM, CO, ozone, and aerosol scattering coefficient were 1.52 (0.165) ng/m³, 142 (14.9) ppbv, 78 (7.7) ppbv, and 3.0 (1.8) Mm⁻¹, respectively. GEM and CO were correlated in the high ozone mode ($r^2 = 0.30$) but were uncorrelated in the lower mode ($r^2 = 0.05$). Three flights observed enhancements of GEM and CO with good correlations and with regression slopes (0.0067 (± 0.0027) ng/m³/ppbv by ordinary least squares regression and 0.0097 (± 0.0018) ng/m³/ppbv by reduced major axis regression) slightly higher than previous observations of enhancements due to Asian industrial long-range transport (LRT). The influence of Asian LRT is supported by back trajectories and a global chemical transport model. In the Seattle-Tacoma boundary layer flight, CO was uncorrelated with GEM, which reflects relatively weaker local GEM sources. On three flights, pockets of air were observed with strong inverse GEM-ozone and ozone-CO correlations (in contrast to all data), which is evidence of upper tropospheric/lower stratospheric (UTLS) influence. An extrapolation of the GEM-CO and GEM-ozone slopes suggests the UTLS can be depleted of GEM.

Citation: Swartzendruber, P. C., D. Chand, D. A. Jaffe, J. Smith, D. Reidmiller, L. Gratz, J. Keeler, S. Strode, L. Jaeglé, and R. Talbot (2008), Vertical distribution of mercury, CO, ozone, and aerosol scattering coefficient in the Pacific Northwest during the spring 2006 INTEX-B campaign, *J. Geophys. Res.*, 113, D10305, doi:10.1029/2007JD009579.

1. Introduction

[2] It has been well established that mercury is a potent neurotoxin that is transported globally in the atmosphere and ocean and bioaccumulates to levels which are toxic for humans and animals at the top of the food chain. The distribution of gaseous mercury in the atmosphere remains a significant uncertainty in our understanding of its global cycle. While there are an increasing number of surface-based observations of mercury, there are a very limited number of observations from aircraft or in the free troposphere. Our uncertainty in the vertical distribution of

mercury is important because the vertical distribution reveals the influence of surface sinks and sources and describes the burden that is available for transport. The uncertainty in the mechanisms controlling the transformation between the species is also critical because oxidation in the free troposphere followed by wet and dry deposition is believed to be the dominant sink of atmospheric mercury [Schroeder and Munthe, 1998; Lin et al., 2006].

[3] Atmospheric mercury is generally divided into three operationally defined fractions: gaseous elemental mercury (Hg_(g)⁰ or GEM), which is the dominant fraction in the troposphere; reactive gaseous mercury (RGM), which is believed to be one or more divalent compounds such as HgO, or HgCl₂; and particulate-bound mercury (PHg), which is mercury in an unknown chemical form that is associated with particulate matter. Knowledge of the speciation is important because of the different fates of each species. RGM is water soluble and is rapidly deposited to surfaces and sequestered by rain and cloud drops. Particulate mercury is limited to the lifetime of the particles which is typically less than 10 d. GEM is not rapidly lost to surfaces and is believed to have a mean global lifetime of

¹Department of Atmospheric Sciences, University of Washington, Seattle, Washington, USA.

²Interdisciplinary Arts and Sciences, University of Washington-Bothell, Bothell, Washington, USA.

³Air Quality Laboratory, University of Michigan, Ann Arbor, Michigan, USA.

⁴Institute for the Study of Earth, Oceans, and Space, University of New Hampshire, Durham, New Hampshire, USA.

0.7–1.7 years controlled primarily by OH oxidation [Selin *et al.*, 2007].

[4] The earliest airborne studies of mercury reported slightly higher concentrations over Europe ($2.24 \pm 0.51 \text{ ng/m}^3$) [Stemr *et al.*, 1985], than are assumed to be the modern northern hemispheric background ($1.3\text{--}1.9 \text{ ng/m}^3$) [Selin *et al.*, 2007]. More recent airborne studies using automated cold-vapor atomic fluorescence spectroscopic (CVAFS) techniques have shown similar, but generally lower concentrations in the free troposphere. Ebinghaus and Stemr [2000], Banic *et al.* [2003], and Friedli *et al.* [2004] reported concentrations ($1.4\text{--}2.3 \text{ ng/m}^3$) in the free troposphere near the northern hemispheric background with minimal vertical trend. In the boundary layer all three studies observed strong enhancements over the free tropospheric values which were attributed to local sources.

[5] In the Pacific Northwest, Weiss-Penzias *et al.* [2003] studied ambient mercury speciation at the Cheeka Peak Observatory (480 m above mean sea level (amsl)) about 2 km inland of the Pacific Coast to the south of the Strait of Juan de Fuca. They observed monthly mean GEM concentrations close to the northern hemispheric background with multiple enhancement and loss events. Some of the enhancements were positively correlated with CO and were attributed to Asian long-range transport (LRT) while others were inversely correlated with CO that had local sources. They hypothesized that mercury could be rapidly lost in anthropogenic pollution, but could not rule out other mechanisms.

[6] At the Mt. Bachelor Observatory (MBO) (Oregon, 2.7 km amsl), Jaffe *et al.* [2005], Weiss-Penzias *et al.* [2006], and Weiss-Penzias *et al.* [2007] analyze observations of Asian industrial LRT, biomass burning plumes, and regional anthropogenic emissions. They identify well correlated GEM and CO enhancements which can be meteorologically linked to the East Asian region and have slopes (or enhancement ratios (ERs)) which agree with each other ($0.003\text{--}0.007 \text{ ng/m}^3/\text{ppb}$) and are about a factor of two greater than estimated Asian anthropogenic emission ratios. Swartzendruber *et al.* [2006] report on the observations of mercury speciation at MBO and note that strong enhancements of RGM are often observed in dry, descending air and cannot be linked to recent anthropogenic emissions. The RGM enhancements are nearly quantitatively correlated to decreases in GEM which suggests that speciation shifts are present in the upper free troposphere or stratosphere.

[7] The ERs from biomass burning as reported by Friedli *et al.* [2004], Weiss-Penzias *et al.* [2007], and Ebinghaus *et al.* [2007] from sources in Asia, continental U.S., Alaska, South America, and South Africa are nearly always lower than industrial ERs from East Asia and Europe. Friedli *et al.* [2004] report Asian industrial ERs as being about 9 times greater than temperate wildfire ERs. Weiss-Penzias *et al.* [2007] report industrial East Asian LRT events with ERs about 2–5 times greater than biomass burning ERs. Stemr *et al.* [2006] report ERs in plumes emanating from Europe as being nearly identical to ERs from industrial East Asian sources.

[8] There have been several aircraft studies of trace gasses in the Pacific Northwest, i.e., Kotchenruther *et al.* [2001], Snow *et al.* [2003], Price *et al.* [2003], Parrish *et al.* [2004], Price *et al.* [2004], Bertschi *et al.* [2004], and

Bertschi and Jaffe [2005], which focused on Asian LRT and the photochemical budget of ozone. Above the boundary layer ($> \sim 2 \text{ km}$) most of these studies observed distinct layers with elevated concentrations of Asian anthropogenic combustion tracers, Siberian or southeast Asian biomass burning, and regional biomass burning. The correlations between CO, O₃, and aerosol scattering coefficient in LRT events were generally good with some variation in the slopes of the enhancement correlation depending on transport height and other constituents such as mineral dust. Also, air masses transported in the upper troposphere were observed to often have characteristics of stratospheric influence [Price *et al.*, 2004].

[9] Our aircraft sampling campaign was concurrent with the second part of NASA's INTEX-B experiment which is the second phase of its INTEX-NA program. The goals of INTEX-B were to understand the transport and transformation of gases and aerosols on intra and intercontinental scales and their impact on air quality and climate. The second part of INTEX-B focused on transpacific transport and evolution of Asian pollution en route to North America. Further information is available at <http://cloud1.arc.nasas.gov/intex-b/>.

[10] In this paper we investigate the vertical profile of mercury in the inflow to the Northwest U.S. based on the following questions:

[11] 1. What is the vertical profile of GEM during the spring in the inflow to the Pacific Northwest?

[12] 2. How is the vertical profile of GEM influenced by long-range transport of Asian anthropogenic emissions?

[13] 3. How does the vertical distribution of GEM relate to the vertical distribution of CO, ozone, and aerosol scattering coefficient and to other air mass types (e.g., LRT, marine, continental, and stratospherically influenced)?

2. Methods

2.1. Region and Flight Plan

[14] Following an initial test flight on 23 March, eight flights were conducted over the Pacific Northwest (Figure 1) between 12 April and 15 May 2006 in order to be approximately concurrent with NASA's INTEX-B campaign. The flight dates and other information are listed in Table 1. The aircraft used was a twin-engine Beechcraft Duchess 76, which has been previously described by Price *et al.* [2003] and Bertschi *et al.* [2004]. Flights were based out of Paine Field (Everett, Washington) and generally followed a pattern of heading due west along the Strait of Juan de Fuca while climbing to the aircraft ceiling of about 5.5–6 km (amsl). Upon reaching the Pacific coast, a vertical “step” profile was taken and the plane then returned to Paine Field at a lower altitude. Flights 4 (30 April) and 8 (15 May) followed this pattern but headed southwest to the Pacific Coast near the border with Oregon, where, on Flight 8, an intercomparison was performed with the INTEX-B DC-8. Flight 5 (4 May) varied significantly from the typical pattern in order to observe anthropogenic pollution in the Seattle and Puget Sound region. This flight followed a “figure eight” pattern around and between Seattle and Tacoma, Washington, at an altitude of less than 500 m above ground level. Lower free tropospheric air (850 to $\sim 700 \text{ mb}$) was sampled at the beginning and end of the

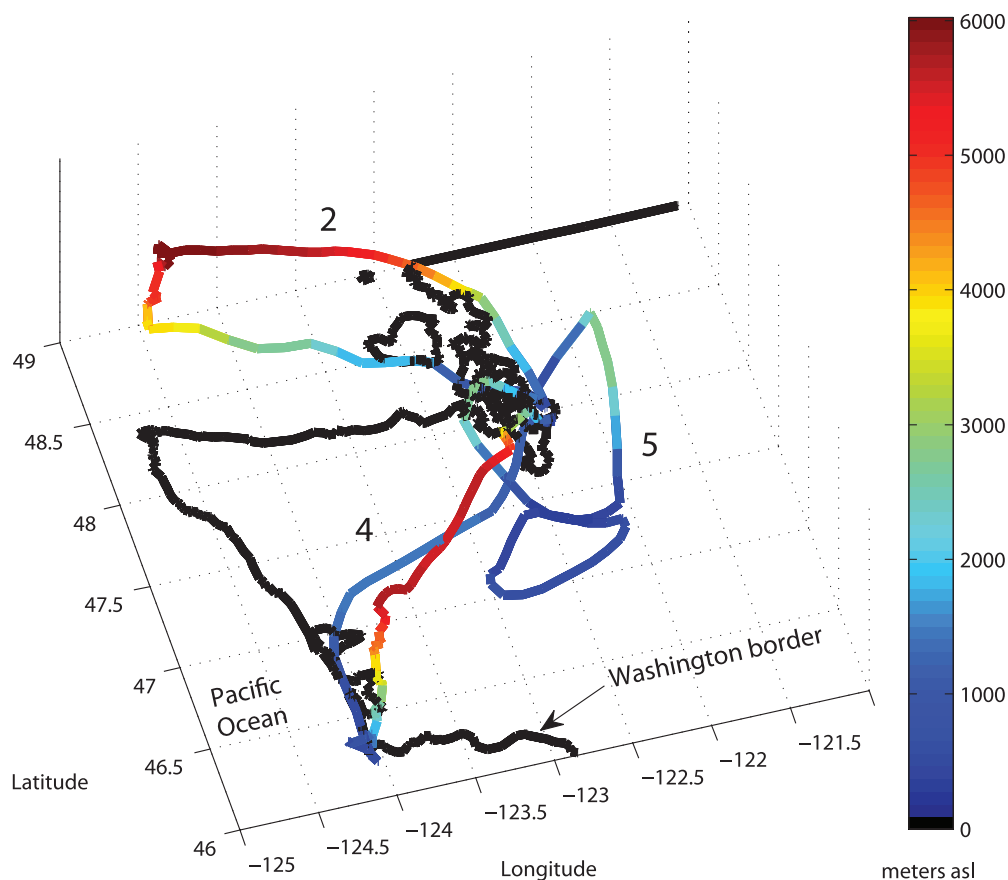


Figure 1. Map of western Washington and three representative flight tracks colored by altitude. Flights 1, 3, 6, and 7 were similar to Flight 2, and Flight 8 was similar to Flight 4.

flight in order to obtain a background for the current synoptic conditions. Three illustrative flight tracks, colored by altitude, are shown in Figure 1, with labels corresponding to the flight number which followed that track. Most of the flight dates were chosen to correspond to the enhanced Asian LRT as predicted by the GEOS-Chem global chemical transport model. The GEOS-Chem model and its application to mercury are described by *Selin et al.* [2007] and *Strode et al.* [2008].

2.2. Instruments

[15] The sampling platform included temperature and relative humidity from a Vaisala HMP45 probe and position and altitude from a handheld Trimble GPS. The chemical measurements included CO, ozone, aerosol scattering coefficient, and mercury. All data, except for mercury, were stored at 1 Hz. CO was measured with a fast response instrument (Aerolaser 5002) based on ultraviolet resonance-fluorescence. The instrument was calibrated using multiple standards (including NIST) prior to the flight, during and after each flight at a time interval of 15–30 min. For a 10-s sample, the detection limit is <2 ppbv, and the total estimated uncertainty (accuracy and precision) is 5%. Ozone was measured with a 2B Technologies miniature UV absorption analyzer. Before most flights, the calibration of the ozone analyzer was verified in the laboratory with an EPA certified O₃ calibration unit according to standard EPA procedures. The total uncertainty (precision and accuracy) is

the greater of ± 4 ppb or 3% for 10 s averages with an estimated detection limit of about 12 ppb. Aerosol scatter (σ_{sp}) was measured with a three-wavelength TSI 3563 integrating nephelometer which was calibrated using CO₂ in particle free air in the laboratory before and after each flight. Zeros were measured just before and after each flight. The detection limit is about 0.6 Mm^{-1} , and the total uncertainty is about 10% [*Chand et al.*, 2006]. Like the ozone analyzer, the nephelometer's calibration constants were also stable, and same value was applied to all flights. This instrument measures the total as well as backscattered signal at three wavelengths (450, 550, 700 nm). Here we report the total scattering coefficient at 550 nm. The inlet was a rear-facing sharp-edged stainless steel tubing which was connected to the nephelometer with 1/2" tube and about 1.5 m length of conductive polymer tubing. Previous studies using this instrument and inlet have determined that this inlet has a cut point of about $0.7 \mu\text{m}$ aerodynamic diameter [*Price et al.*, 2003]. The scattering coefficient values have been corrected to standard temperature and pressure for all of the described analysis. The ozone, CO, and aerosol scattering data were averaged to the 2.5 min sample periods of the mercury instrument.

2.3. Mercury

2.3.1. Instrument

[16] Mercury was measured with a Tekran 2537A cold-vapor atomic fluorescence (CVAFS) instrument. The instru-

Table 1. Summary of Flight Number, Date, Day of Year, and Comment for Each Flight

Flight Number	Date	Day of Year (DOY)	Comment
1	12 Apr	102	influence of Asian LRT 630–500 mb
2	18 Apr	108	influence of Asian LRT 730–480 mb, up. trop. influence 650–500 mb
3	19 Apr	109	profile very similar to 18 Apr
4	30 Apr	120	profile at southwest WA coast
5	4 May	124	Seattle & Tacoma boundary layer flight, up. trop. influence 780–730 mb
6	8 May	128	influence of Asian LRT 600–470 mb, up. trop. influence 540–500 mb
7	9 May	129	lower GEM in mixed layer
8	15 May	135	intercomparison with DC-8 at SW WA coast

ment employs parallel Au cartridges which alternately collect GEM and quantify the collected mercury by thermal desorption into a carrier gas (UHP Ar) which is quantified by CVAFS. For this study, the collection and desorption cycle was set to 2.5 min and the data are reported as ng/standard m³. The detector is regularly calibrated by referencing an internal temperature-controlled permeation tube which was certified by the manufacturer to $\pm 10\%$. The stability and accuracy of the permeation tube is challenged by injections of saturated GEM vapor from a temperature controlled (NIST traceable) primary vapor source (Tekran 2505). The instrument was calibrated from the permeation tube multiple times immediately prior to each flight and was also challenged with manual injections before and after most flights. The ambient pressure change in-flight temporarily perturbed the effective permeation rate of the tube immediately after each flight, but in all cases it returned to its preflight rate within about 24–48 h. In 12 sets of permeation-injection comparisons interspersed between flights, the permeation tube calibration agreed with the manual injection calibrations with a mean relative percent difference (RPD) ($\pm 1 - \sigma$) of 2.2% ($\pm 1.9\%$) with the standard deviation of successive permeation calibrations being $\pm 1.7\%$. The permeation rate measured at the end of the campaign agreed with the value measured at the beginning of the campaign to better than 1% RPD. The detection limit is estimated to be 0.1 ng/m³ based on 3x the standard deviation of stable, low concentration data.

[17] The total uncertainty for the 2537 (without considering pressure correction effects which will be discussed in the following paragraphs) is estimated from the uncertainty in the primary (injection) standard of 1.8% (Tekran [2006] and uncertainty in our syringe volume), a conservative estimate of the uncertainty (precision and accuracy) of the agreement with the working (permeation) calibration standard of 4.1%, and the uncertainty in the sample volume of 1%. The total uncertainty (root sum of squares of 1.8%, 4.1%, and 1%) of our GEM data at constant ambient pressure is 5%.

2.3.2. Inlet and Sample Line

[18] The mercury inlet was a rear-facing, 1/4" Teflon tube about 20 cm in length which bent 90° to enter the aircraft. Immediately inside the aircraft, a KCl trap was attached to scrub the stream of any reactive oxidized species which may be present in the free-troposphere [Landis *et al.*, 2005; Swartzendruber *et al.*, 2006]. The KCl trap was composed

of quartz chips coated with a KCl solution and packed into a 1/2" Teflon tube and held in place with quartz wool. The quartz chips and KCl solution were taken from the same stock used for concurrent Hg speciation measurements at MBO with an automated Tekran speciation system described by Swartzendruber *et al.* [2006]. Before and after each flight, the entire sample line was leak and blank tested and no significant GEM artifact was observed from the KCl trap.

[19] The use of a KCl trap ensures that the values reported by the Tekran 2537 unambiguously represent only GEM. While it has been assumed there is little RGM in the free-troposphere, recent observations have challenged that assumption [Landis *et al.*, 2005; Swartzendruber *et al.*, 2006]. In the laboratory, we tested the Tekran 2537's direct sensitivity (without a KCl trap) to an RGM proxy (HgCl₂) at a concentration of 580 pg/m³ (as measured by a KCl denuder). We found a recovery of $-4.5\% \pm 11\%$ (95% confidence interval) which argues that a typical 2537 sampling configuration has no significant sensitivity to RGM even at very high concentrations. The RGM present in the test atmosphere was either not quantitatively transmitted to the 2537 (through 1 m of 1/4" Teflon tubing with no filter pack) or through the 2537 or could not be detected

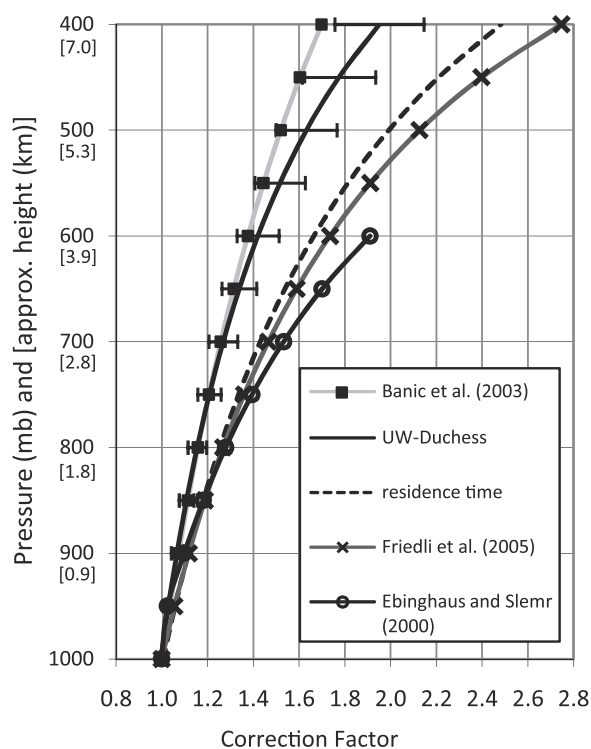


Figure 2. The average pressure correction factors used for our data (with error bars representing uncertainty) along with those of Ebinghaus and Slemr [2000], Banic *et al.* [2003], and Friedli *et al.* [2004] and a fluorescence cell residence time correction factor for reference. Note that the pressure sensitivities reported by Ebinghaus and Slemr [2000] and Friedli *et al.* [2004] were determined with different techniques and may not necessarily be comparable to Banic *et al.* [2003] and to our results. See section 2.3.3 for further details.

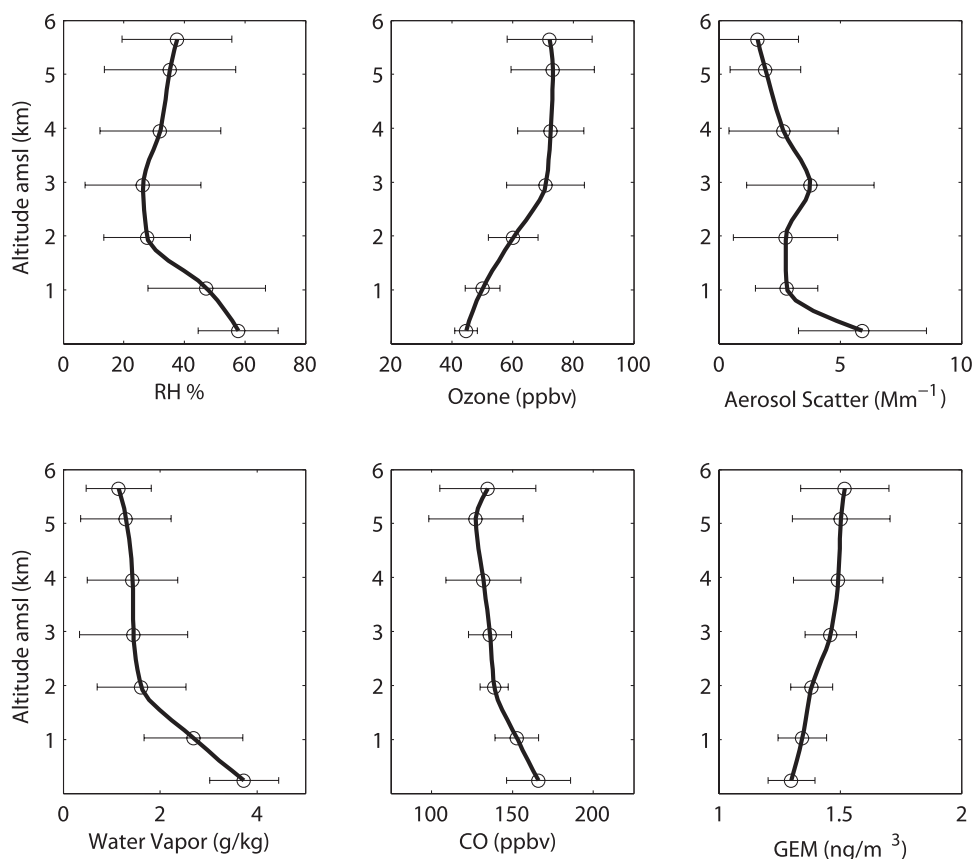


Figure 3. Mean profile of all flights binned ± 0.5 km from plotted point. This does not include Flight 5 (4 May) which sampled the Seattle-Tacoma boundary layer. The error bars are one standard deviation within the respective bin.

by thermal desorption and CVAFS at 253.7 nm. The fate of the HgCl_2 in the line or in the 2537 is not known and could be dependent on RH (e.g., *Temme et al.* [2003] report sensitivity to RGM at low RH) or other factors (E. Prestbo, personal communication, 2007) and has the potential to generate artifacts.

2.3.3. Pressure Correction

[20] The sensitivity of the Tekran 2537A to ambient pressure has been discussed in several studies [*Ebinghaus and Slemr*, 2000; *Banic et al.*, 2003; *Friedli et al.*, 2004]. While changes in sensitivity can theoretically be corrected by appropriate in situ calibration, the changes encountered during aircraft studies are too rapid for this to be practical. Therefore, aircraft observations must either control the pressure of the fluorescence cell or apply an empirical correction factor which is dependent on the ambient pressure. We determined a pressure correction factor in the laboratory by placing the cell vent under vacuum and performing repeated permeation calibrations.

[21] Figure 2 shows the average pressure correction factor determined in two lab tests compared with the results from three other studies, [*Ebinghaus and Slemr*, 2000; *Banic et al.*, 2003; *Friedli et al.*, 2004]. Our correction factor function fit the data with $r^2 > 0.999$ and takes the form $\text{CF}(p) = A + B/p$ where p is the pressure and A and B are empirically determined constants. Each test was comprised of six or seven points that spanned from 1000 mb to about 300 mb. The vacuum sensitivity test was performed three

times. The first test used ambient air as the mercury source, but the concentrations were not stable enough for the correction factor to be measured with high confidence. So, when the test was repeated in the middle and end of the campaign, the internal permeation tube (which was not connected to the vacuum) was used as the mercury source. We estimate the uncertainty in the correction factor using the A and B cartridges at each pressure point from the second and third tests ($n = 4$). The relative standard deviation (RSD) of the measured correction factors (which is an estimate of the $1 - \sigma$ uncertainty) increased as a function of pressure from 0.4% at 1013 mb to 2.7% at 400 mb. We then conservatively apply the Chi-square statistic to obtain the upper 95% confidence limit on the true standard deviation (i.e., on the true $1 - \sigma$ uncertainty). This yields a pressure correction uncertainty that ranges from 1.3% at the surface to 10% at 400 mb and is plotted as error bars in Figure 2. Combined with the uncertainty of the mercury quantification, the total uncertainty for our GEM data varies from 4.8% at the surface to 11% at 400 mb.

[22] The changing sensitivity of the instrument with ambient pressure, to a first approximation, is due to the changing residence time of the desorbed Hg atoms in the fluorescence cell, which can be deduced as follows. First, we note that the concentration of the fluorescing atoms is very dilute (therefore self interactions are negligible) and the fluorescence lifetime of an Hg atom (~ 100 ns) is much shorter than its residence time in the cell. Since the signal

Table 2. Statistical Summary of All Data Binned by Altitude Segment

	Temperature, C	RH, %	H ₂ O, g/kg	Ozone, ppbv	σ_{sp} , Mm ⁻¹	CO, ppbv	GEM, ng/m ³
5.5–6.5 km Mean	-13.6	38	1.1	72.3	1.59	135	1.52
Std. Dev.	3.81	18	0.67	14.0	1.69	29.6	0.182
Min	-19.1	10	0.18	46.2	0.10	74.0	1.17
Max	-5.70	71	3.2	112	8.3	174	2.02
Median	-14.9	38	1.0	75.4	0.71	147	1.56
n	66	66	66	66	74	74	68
4.5–5.5 km Mean	-10.6	35	1.3	73.3	1.92	127	1.50
Std. Dev.	4.20	22	0.93	13.7	1.46	29.0	0.201
Min	-19.9	7.0	0.16	43.4	0.10	71.3	1.12
Max	0.70	84	4.5	108	5.9	174	2.02
Median	-11.5	32	1.1	74.2	1.82	135	1.49
n	98	98	98	100	112	110	106
3.5–4.5 km Mean	-5.40	32	1.4	72.6	2.67	132	1.49
Std. Dev.	4.09	20	0.93	11.0	2.24	23.3	0.184
Min	-12.7	10	0.30	41.4	0.10	76.3	1.16
Max	6.90	76	3.7	91.1	8.7	172	1.93
Median	-6.45	24	1.2	73.9	2.00	137	1.49
n	58	58	58	59	64	64	56
2.5–3.5 km Mean	-0.66	24	1.3	72.4	3.63	136	1.45
Std. Dev.	4.93	19	1.12	13.0	2.55	12.8	0.113
Min	-9.90	2.4	0.18	37.7	0.10	116	1.20
Max	13.0	85	3.7	94.0	10.4	165	1.72
Median	-1.80	21	0.9	76.8	3.67	136	1.44
n	66	66	66	70	74	73	67
1.5–2.5 km Mean	2.39	27	1.6	60.6	2.86	139	1.38
Std. Dev.	5.54	14	0.90	8.13	2.12	8.5	0.087
Min	-4.20	4.5	0.28	40.8	0.42	112	1.22
Max	17.1	76	3.5	77.2	11.4	156	1.60
Median	0.75	23	1.5	59.3	2.05	139	1.37
n	62	62	62	64	69	69	65
0.5–1.5 km Mean	5.59	43	2.7	50.4	3.35	155	1.34
Std. Dev.	5.01	20	0.94	5.49	1.94	14.8	0.095
Min	-0.90	5.1	0.30	41.4	0.10	118	0.99
Max	20.5	77	4.3	73.7	9.36	199	1.56
Median	3.90	45	2.8	49.4	2.68	152	1.33
n	97	97	97	101	104	100	97
0–0.5 km Mean	12.1	39	3.2	47.9	6.63	169	1.30
Std. Dev.	5.05	21	0.76	4.96	2.24	20.6	0.084
Min	4.80	17	2.2	33.4	1.74	140	1.16
Max	19.3	80	4.7	56.4	11.2	214	1.52
Median	13.6	31	2.9	47.3	6.60	166	1.30
n	34	34	34	39	40	37	35
All data Mean	-2.47	34	1.8	64.7	2.95	140	1.43
Std. Dev.	9.21	20	1.1	14.9	2.36	24.7	0.166
Min	-19.9	2.4	0.16	33.4	0.10	71.3	0.994
Max	20.5	85	4.7	112	11.4	214	2.02
Median	-2.70	30	1.6	64.5	2.29	143	1.41
n	481	481	481	499	537	527	494

reported by the 2537 is a time integral over a peak, the particular shape of the peak and therefore the timing of the passing of the atoms through the cell is unimportant for the purpose of quantification. This means that the number of atoms in the cell at any particular time (number density) is unimportant; only the total number of atoms which pass through the cell and the average time they spend in the cell are important. The total area can be simply expressed as the product of the total number of fluorescing atoms, their average residence time in the fluorescence cell, and a constant that describes the fluorescence emittance rate per atom. A correction factor for only the residence time effect is also plotted in Figure 2.

[23] There also appear to be additional, higher-order effects on the sensitivity. These effects are apparent when comparing the observed vacuum correction factor (Figure 2)

with the theoretical correction factor based solely on fluorescence cell residence time. The difference between these two values fits ($r^2 = 0.998$) the Stern-Volmer equation for fluorescence quenching. This suggests that the detector sensitivity, when corrected for cell residence time, actually increases slightly with decreasing pressure as would be expected from reduced fluorescence quenching. Although the Stern-Volmer equation fits this effect, this does not mean that fluorescence quenching is necessarily responsible as other effects can take the same form [Mitchell and Zemansky, 1971].

[24] Our results are similar to those of Ebinghaus and Slemr [2000], Banic et al. [2003], and Friedli et al. [2004] in suggesting that the ambient pressure is an important variable that affects the instrument's sensitivity. Since these groups used different techniques to estimate the pressure dependency (Friedli et al. [2004] extrapolated from calibrations at 1020 and 823 mb, and Ebinghaus and Slemr [2000] performed manual injections into a model 2500 detector), the factors may not be directly comparable to the vacuum technique used by Banic et al. [2003] and by this study. While the correction factors used by all of these groups appear to span a large range (e.g., about 60% at 400 mb) the ambient data obtained using these factors are in much closer agreement. At about 400 mb, Banic et al. [2003] report means of 1.5–1.7 ng/m³, we observed a mean of 1.52 ng/m³ in our highest altitude bin, and Friedli et al. [2004] report concentrations between 1.4 and 2.0 ng/m³ near this altitude. Our tests suggest that quenching may also play a role in the pressure sensitivity. It is plausible that some of the variability in the correction factors could be explained by variability in quenching caused by varying amounts of trace contaminants in the 2537 carrier gas.

2.4. Trinidad Head Ozonesonde Data

[25] Trinidad Head is an Earth System Research Laboratory site (or ESRL, formerly known as CMDL) on the coast of northern California (41.05°N, 124.15°W) where continuous trace gas measurements are made and ozonesondes are launched weekly or more frequently during specific campaigns. The data were obtained from an online archive which can be accessed from NOAA's ESRL site: <http://www.ersl.noaa.gov/gmd/dv/ftpdata.html>. The data are on 100 m interval averages up to 400 mb and were taken from sondes launched on flight days ± 2 d, which are 9 of 14 sondes available during our campaign.

3. Results and Discussion

3.1. Aggregate Data

[26] The mean profiles of RH, water vapor, CO, ozone, aerosol scattering coefficient (σ_{sp}), and GEM for all flights,

Table 3. Pearson's Correlation (r) of All Data

	Pressure	Temperature	RH	O ₃	σ_{sp}	CO	GEM
Temperature	0.87	1					
RH	0.09	-0.04	1				
O ₃	-0.66	-0.66	-0.40	1			
σ_{sp}	0.44	0.51	-0.04	-0.07	1		
CO	0.43	0.21	0.05	0.01	0.49	1	
GEM	-0.48	-0.46	0.19	0.45	0.01	0.31	1
H ₂ O	0.57	0.59	0.73	-0.73	0.32	0.14	-0.15

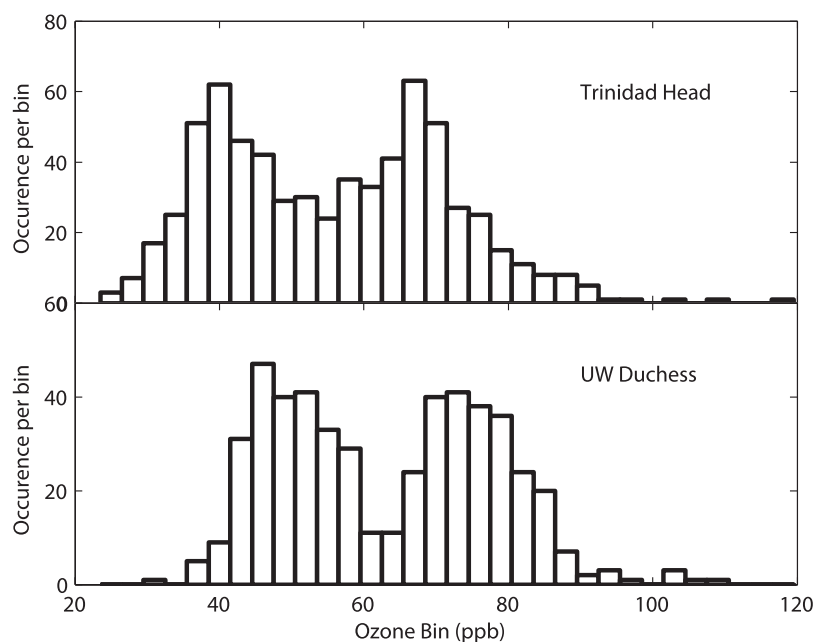


Figure 4. Histograms of ozone from the UW-Duchess aircraft and Trinidad Head ozonesondes at comparable altitudes, during flight days ± 2 d.

except Flight 5 (4 May), are shown in Figure 3 along with their respective standard deviations. Flight 5 (4 May) is excluded because it disproportionately samples the Seattle-Tacoma urban boundary layer and therefore has the potential to bias any summary statistics. The profile data have been binned by altitude (0.5–1.5 km, etc.) and plotted versus the average altitude within each bin. RH, σ_{sp} , water vapor, and CO generally decrease from the surface up to about 2 km as would be expected for substances with surface sources. GEM and ozone show an increase up to about 2–3 km and are nearly constant above this level. Several flights had notable deviations from these general patterns and will be analyzed on a case-by-case basis. The mean, median, standard deviation, minimum and maximum, and number of 5-min samples in each altitude are listed in Table 2.

3.1.1. Correlations

[27] Pearson's correlation coefficients (r) are shown in Table 3 for all data. The strongest correlations in the overall data are between σ_{sp} and CO (0.49), GEM and CO (0.31), and GEM and ozone (0.45) ($p < 0.0001$ for all). The positive correlations between σ_{sp} , CO, and GEM are consistent with influence from anthropogenic emissions and biomass burning.

3.1.2. Comparison to Previous Flights

[28] Measurements of ozone, CO, and σ_{sp} were performed on previous flights in the Pacific Northwest in 1999, 2001–2002, and in a 2003 study of biomass smoke [Kotchenruther *et al.*, 2001; Price *et al.*, 2003; Bertschi *et al.*, 2004; Bertschi and Jaffe, 2005]. The mean ozone concentrations we observed above about 3 km (~ 73 ppbv) are similar to those observed in 1999 (60–80 ppbv) but are higher than observed in 2001, 2002, and 2003 (~ 45 , 57, and 59 ppbv, respectively). The greatest difference is in comparison with 2001 in which there was little variation in the mean ozone mixing ratios from the surface to 6 km.

[29] We observed mean CO concentrations above 3 km of about 140 ppbv which is very similar to the flights in 1999 (~ 140 ppbv), 2001 (~ 135 ppbv), and 2002 (~ 140 ppbv), but is higher than observed in the 2003. While the 2003 flights detected much higher mixing ratios of CO in Asian boreal fire plumes, outside of these events, CO mixing ratios were much lower (~ 100 ppbv) as most of the flights were in June and July when background concentrations are typically lower.

[30] The mean and median σ_{sp} values we observed (2–3 Mm^{-1}) are also very similar to the median values seen in all four previous aircraft campaigns. The most salient difference is the higher mean σ_{sp} values observed in 2001, 2002, and 2003 due to layers of long-range transported anthropogenic and biomass burning plumes with σ_{sp} values as high as 41, 65, and 100 Mm^{-1} , respectively.

3.1.3. Gaseous Elemental Mercury

[31] We observed gaseous elemental mercury concentrations (in $ng/standard\ m^3$ which is independent of pressure like a mixing ratio) in the upper altitudes in agreement with surface studies at Cheeka Peak, observations in the free troposphere at MBO, and other airborne studies [Banic *et al.*, 2003; Ebinghaus and Slemr, 2000]. The mean concentrations in our upper altitude (>2.5 km) bins ranged from 1.45 to 1.52 ng/m^3 . The mean concentrations in the lower altitude bins were somewhat lower and ranged from 1.30 to 1.38 ng/m^3 .

[32] Studies of mercury at MBO (~ 730 hPa) in April–May of 2004 found mean total airborne Hg concentrations (and standard deviation) of 1.77 (0.12) ng/m^3 [Jaffe *et al.*, 2005]. Subsequent studies of speciated mercury at MBO found nighttime (which is more representative of the free troposphere) concentrations of GEM in May–August 2005 of 1.51 (0.196) ng/m^3 [Swartzendruber *et al.*, 2006]; in April–June 2006, 1.56 (0.194) ng/m^3 ; and in April–July 2007, 1.50 (0.224) ng/m^3 . Note that the 2004 data should be

Table 4. Pearson's Correlation (r) and Mean Mixing Ratio of Key Parameters Segregated by Ozone Into Higher (>63 ppbv) and Lower (<63 ppbv) Modes

	Pearson's Correlation			Mean Mixing Ratio ^a			
	(r)			O ₃	σ_{sp}	CO	GEM
	GEM-O ₃	GEM-CO	GEM-RH				
All data ^b	0.35	0.22	0.19	65.8	2.90	143	1.46
Higher mode ^c	-0.22	0.54	0.52	77.7	3.00	142	1.52
Lower mode ^b	0.19	-0.18	0.04	51.3	2.77	145	1.39
Significance ^d p	-	-	-	<0.0001	0.273	0.093	<0.0001

^aUnits are ppbv, Mm⁻¹, ppbv, and ng/m³, respectively.

^bDoes not include Flight 5.

^cDoes not include outlying CO values from Flight 8 (15 May).

^dSignificance of the difference between the means of the higher and lower modes.

considered an upper limit and may not be directly comparable because the method did not separate RGM and particulate-bound mercury but pyrolytically converted all species to the elemental form.

[33] Our results above 2.5 km (1.45 to 1.52 ng/m³) are in agreement with those reported by *Ebinghaus and Slemr* [2000] at 2500 masl (1.64 \pm 0.094 ng/m³) and by *Banic et al.* [2003] (1.3 to 1.6 ng/m³) in their flights on the coast of Nova Scotia. *Friedli et al.* [2004] reported slightly higher concentrations of GEM in the Western Pacific along with enhanced CO and attributed these elevations to the outflow of anthropogenic pollution from industrial East Asia.

[34] Below 2.5 km, we observed significantly lower mean GEM concentrations than reported by *Ebinghaus and Slemr* [2000] (2.19 and 2.32 ng/m³) and by *Friedli et al.* [2004] (1.8–2.0 ng/m³), both of which were considered elevated due to local sources. Our results are, however, very similar to aircraft observations of *Banic et al.* [2003] who report GEM modes of 1.3 and 1.4 ng/m³ in altitude sections of <1 km and 1–3 km, respectively, near the coast of Nova Scotia. When our data are binned identically, we observed GEM modes of 1.4 ng/m³ in both altitude sections. The only important difference is that they observed a skewed upper tail at altitudes <1 km, which they attributed to local sources. In comparison to surface studies at the Cheeka Peak Observatory (which is on the Pacific coast at the western end of the flight paths of Flights 1, 2, 3, 6, and 7) *Weiss-Penzias et al.* [2003] found minimally higher seasonal mean GEM concentrations of 1.46–1.50 ng/m³ in continental air, and 1.51–1.64 ng/m³ in marine air.

3.2. Bimodal Distribution of Ozone

[35] The most salient feature of the aggregate data set is a strong bimodal distribution of ozone. A histogram of the aircraft ozone observations is shown in Figure 4 along with comparable data from nine Trinidad Head ozonesondes using the same bin intervals. A strong bimodal distribution is also observed in the Trinidad Head data which were taken from sondes launched on flight days ± 2 d. The bimodal pattern is believed to be a robust feature as it is seen in the histogram of all 14 sondes available during our campaign.

[36] The altitude dependence of the two modes can be seen by segregating the modes at the minimum between them (63 ppbv) and plotting the distribution of the higher and lower modes at each altitude level (figure not shown).

About 14% of the ozone values above 2.5 km are from the lower ozone mode, but these are almost entirely from an isolated pocket of background air observed in Flight 8 (15 May). The CO concentrations in this air (70–80 ppbv) were much lower than the median (143 ppbv) and are well below 1.5x the interquartile range of the CO distribution and are considered outliers. These points have been removed from the lower-ozone mode for all subsequent statistical analysis. The two modes of the Duchess ozone data are consistent with a division between the free troposphere and mixed layer which occurs between 2 and 3 km as can be seen in the water vapor and CO profiles shown in Figure 3.

[37] A bimodal distribution requires that significantly different sources perturb the boundary layer and lower free-troposphere on a timescale that is more rapid than mixing can occur. *Holzer and Hall* [2007] show evidence of a similar phenomenon occurring in transpacific transport. They report that in the 1999–2001 summertime Pacific troposphere, transport above and below 2.2 km form distinct modes due to strong stability and weak baroclinicity. While our observations are in the late spring, it seems plausible that similar high-stability conditions and a similar separation could have been present. The lower and middle troposphere (2.5–6 km) could have enhanced photochemical production of ozone due to transport of ozone precursors or stratospheric influence which often accompanies long-range transport at higher altitudes [*Cooper et al.*, 2004], or some combination of both.

3.2.1. Segregated Ozone Modes

[38] The bimodal distribution of ozone forms a natural division to analyze the data set and contrast the differences between the free-troposphere and the mixed layer. Table 4 shows the key differences in correlations and the mean concentrations between the two modes. Note that Flight 5 has been excluded from these statistics. Both the GEM-RH and the GEM-CO correlations are modestly strong in the higher mode but are weakly negative or not significant in the lower mode. The GEM-CO pattern is consistent with greater influence of Asian LRT in the upper mode as local emissions in the lower mode would have a smaller GEM:CO ratio [*Weiss-Penzias et al.*, 2007] which would produce a smaller slope and weaker correlation.

[39] The GEM-ozone correlations change dramatically when the data are separated by ozone mode. In the complete data set, the correlation is weak ($r = 0.35$), but when segregated, the correlation in the higher ozone mode becomes weakly negative, and of marginal significance. In the lower ozone mode, the correlation remains positive, but weakens and also becomes marginally significant. The overall GEM-ozone correlation implies that the boundary layer and surface is a sink for GEM as it is for ozone; however, this correlation is much weaker ($r^2 < 0.04$) in the lower ozone mode which is <2.5 km and is negative in the upper mode. The differing correlations in the upper and lower altitudes (cf. Table 4) argues that although there may be a surface sink of GEM, it is not the dominant influence on the GEM vertical profile in our data and is not needed to explain the overall GEM-ozone correlation. Rather, the overall GEM-ozone correlation can be explained by the upper altitude mode having sources of GEM from Asian

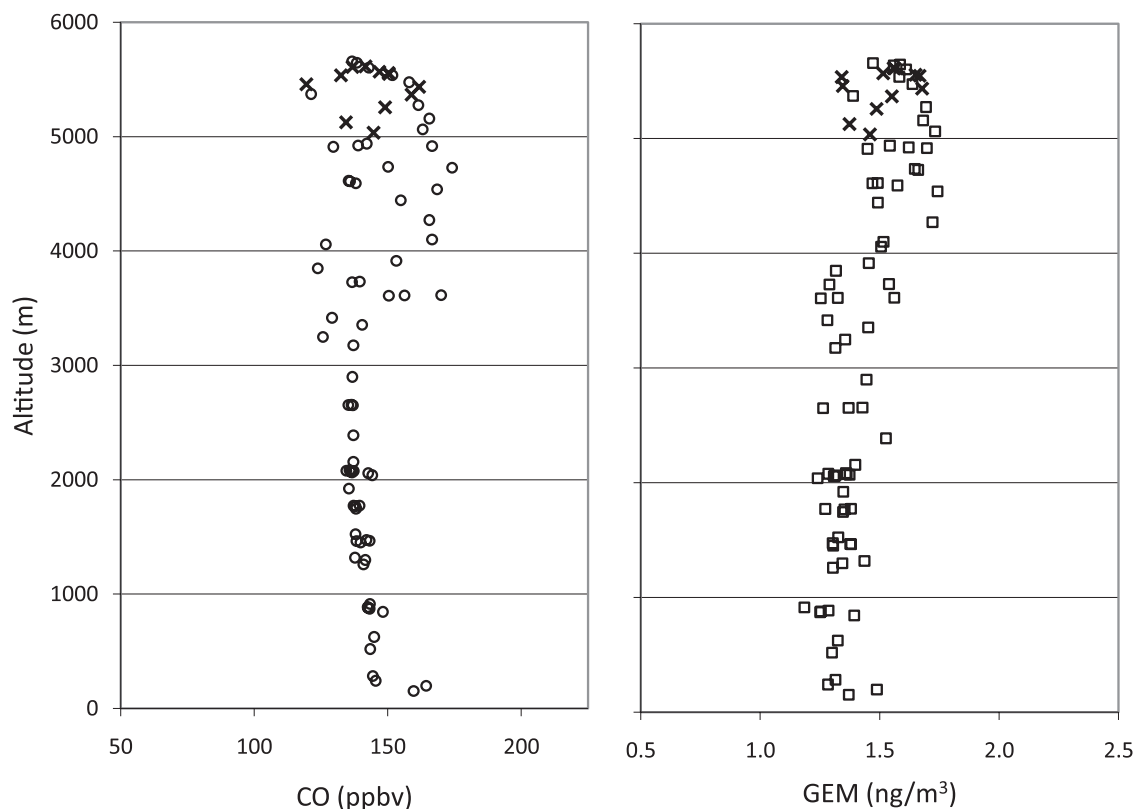


Figure 5. Vertical profiles of CO and GEM from Flight 6 (8 May). Points indicated by bold cross symbols are those with upper-tropospheric influence discussed in section 3.4 and are also plotted in Figure 10.

LRT, and ozone from in situ production or subsidence from the upper troposphere or stratosphere or both.

3.3. GEM-CO Relationship

3.3.1. Influence of Asian Industrial Long-Range Transport Above 2.5 km

[40] The GEM-CO correlation ($r^2 = 0.30$) is the strongest relationship among all chemicals in the high-ozone mode. The correlation is driven by GEM and CO enhancements on three flights which have slopes (ERs) that are similar to previous observations of anthropogenic Asian LRT. The influence of Asian LRT is also supported by kinematic back trajectories and (in section 4.3.2) a GEOS-Chem global chemical transport simulation. The robustness of the ERs is investigated with a second regression technique and estimations of confidence intervals, and the implications are discussed.

[41] An example profile which shows enhancements of GEM and CO in Flight 6 (8 May) is shown in Figure 5. On flights 1 (12 April), 2 (18 April), and 6 (8 May), the GEM-CO ERs were $0.0068 \text{ ng/m}^3/\text{ppbv}$ ($r^2 = 0.34$), $0.0067 \text{ ng/m}^3/\text{ppbv}$ ($r^2 = 0.56$), and $0.0062 \text{ ng/m}^3/\text{ppbv}$ ($r^2 = 0.60$), respectively ($p < 0.005$ for all three), with a mean of $0.0067 \text{ ng/m}^3/\text{ppbv}$ (7.5×10^{-7} in molar units).

[42] Three-dimensional kinematic backtrajectories using NOAA's HYSPLIT model [Draxler and Rolph, 2003] from the three flights are also consistent with the East Asian region being a source of the enhancements. An example from Flight 2 (18 April) is shown in Figure 6 which depicts

nine trajectories ending in the portion of the flight in which the strong GEM:CO correlation (ERs) was observed. All of the trajectories come from the East Asian region and six of them pass over regions with substantial GEM emissions based on global emissions mapping [Pacyna and Pacyna, 2002] and three trajectories emanate from the boundary layer. The trajectories from the two other days with good GEM:CO correlations show a similar path and also have a number of trajectories which reach the boundary layer.

[43] These slopes were determined from ordinary least squares (OLS) regression which may be useful for comparison with previous work but may not be robust for bivariate data with similar magnitude uncertainty in the both parameters [Ayers, 2001]. Therefore, a regression technique that can be more robust with uncertainty in both parameters, reduced major axis (RMA) regression was also performed. RMA regression yielded slopes for the flights 1, 2, and 6 that are, respectively, 0.012, 0.0090, and $0.0082 \text{ ng/m}^3/\text{ppbv}$ with a mean of $0.0097 \text{ ng/m}^3/\text{ppbv}$ (1.1×10^{-6} in molar units). The difference between the RMA and OLS regression lines can be seen for Flight 1 (12 April) in Figure 7. It should also be noted that the slope determined by RMA regression is always greater in magnitude than by OLS [Ayers, 2001] and the difference decreases as r^2 approaches unity.

[44] Confidence intervals for the OLS and RMA slopes are estimated by combining the potential contribution of independent, random errors in GEM (with total uncertainty 4.8–11%) and dependent, systemic uncertainty due to

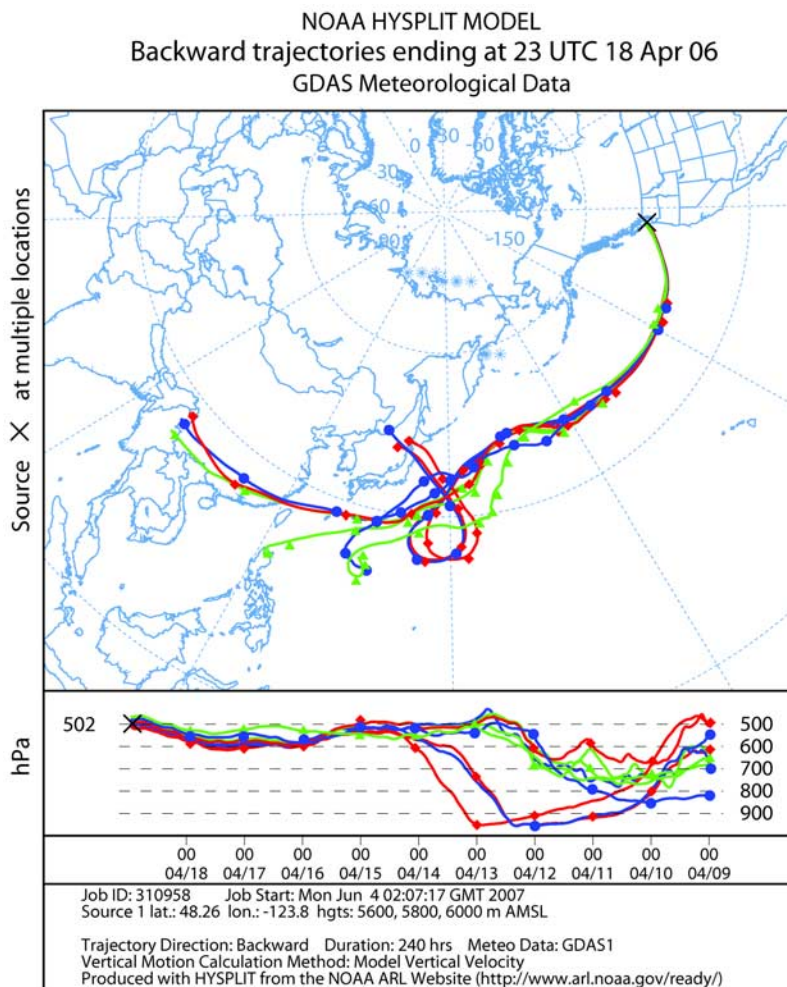


Figure 6. Backtrajectories for Asian LRT event observed on Flight 2 (18 April).

variability in the calibration of the CO (5%) and for GEM, variability in the calibration (4.6%) and pressure correction (10%). Because the independent errors are heteroscedastic (i.e., not constant throughout the range of data) the confidence intervals for the OLS regressions were estimated from a 599 member bootstrap procedure following *Wilcox* [2005]. As there currently is no standard approach that explicitly accounts for heteroscedasticity in RMA regression, these confidence intervals were estimated using 10,000 member percentile bootstraps [Wilcox, 2005]. The uncertainty due to dependent, systemic errors was estimated with a 10,000 member Monte Carlo simulation of simultaneous, random, systemic bias in both CO and GEM.

[45] For OLS regression, the 95% confidence interval in the mean slope is estimated to be $\pm 40\%$ based on combining (root sum of squares) the relative confidence interval due to random error, $\pm 38\%$, and due to systemic error, $\pm 12\%$. Similarly for RMA regression, the 95% confidence interval is estimated to be $\pm 18\%$ ($\pm 14\%$ and $\pm 12\%$, respectively). This yields mean slopes of $0.0067 (\pm 0.0027) \text{ ng/m}^3/\text{ppbv}$ by OLS regression and $0.0097 (\pm 0.0018) \text{ ng/m}^3/\text{ppbv}$ by RMA regression.

[46] Our slopes (within the estimated confidence interval) determined by OLS agree with previous observations of

industrial ERs. *Friedli et al.* [2004] report an ER in the “Shanghai plume” of $0.0080 \text{ ng/m}^3/\text{ppbv}$ observed off the coast of southeast China, *Jaffé et al.* [2005] report a slope of $0.0053 \text{ ng/m}^3/\text{ppbv}$ ($r^2 = 0.84$) for all Asian outflow data at Cape Hedo, Okinawa, JP (HSO), and *Weiss-Penzias et al.* [2007] report a mean Asian industrial ER of $0.0046 (1 - \sigma = \pm 0.0013) \text{ ng/m}^3/\text{ppbv}$ ($r^2 > 0.5$) observed at MBO. *Slemr et al.* [2006] report observing a mean European industrial ER of $0.0050 (1 - \sigma = \pm 0.0021) \text{ ng/m}^3/\text{ppbv}$. Also, our OLS and RMA ERs are greater than those reported by *Ebinghaus et al.* [2007] by a factor 3–10 because their observations are of biomass burning and our observations are of industrial emissions, which have significantly lower ERs [Friedli et al., 2004; Weiss-Penzias et al., 2007].

[47] While our mean RMA regression slope ($0.0097 (\pm 0.0018) \text{ ng/m}^3/\text{ppbv}$) is somewhat greater than the (OLS) industrial ERs described above, it is in agreement to the ratio reported by *Friedli et al.* [2004]. Our ERs do imply an Asian industrial emission ratio that is slightly greater than has been previously reported (discussed above). This carries important implications for Asian emissions so the limitations of this inference must be clearly noted.

[48] First, the quantitative relationship between an observed ER and the actual emission ratio depends on the

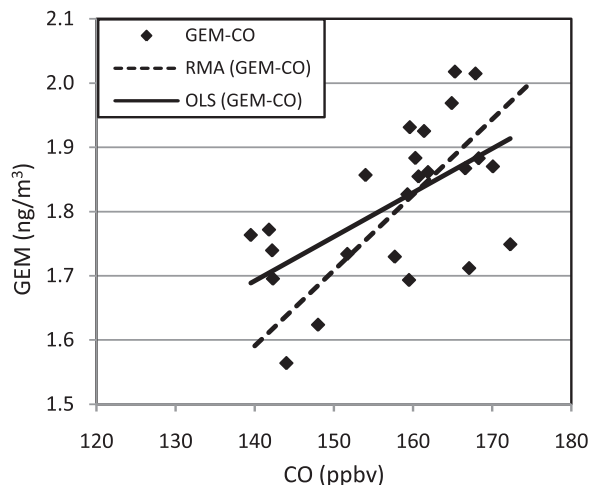


Figure 7. Scatterplot of GEM and CO enhancement in Flight 1 shown with linear or ordinary least squares regression (OLS) and reduced major axis (RMA) regression lines. The OLS and RMA slopes are, 0.0068 ($r^2 = 0.34$) and 0.012 $\text{ng/m}^3/\text{ppbv}$, respectively.

assumptions described by *Jaffe et al.* [2005]. Violations of the assumptions could include changing background concentrations, mixing-in of biomass burning emissions which would lower the ratio, reduction of RGM in the outflow [*Lohman et al.*, 2006], or evolution of the ratio during transport because of different tropospheric lifetimes [e.g., *Carmichael et al.*, 2003]. Second, while RMA regression has been shown to be significantly more accurate in at least some situations [*Draper and Smith*, 1998; *Ayers*, 2001] it is not known if it is appropriate in the present application or how robust it is to violations of the assumptions of relating an observed ER to the actual emission ratio. Third, our mean ER is derived from three events which may not be representative of longer term emissions. Fourth, the influence of other factors (e.g., reemission [*Strode et al.*, 2008]) could be seasonal or changing.

3.3.2. Comparison With GEOS-Chem Chemical Transport Model

[49] The GEOS-Chem model was run with tagged, anthropogenic Asian emissions of GEM and CO. A more complete description of the model and additional results are discussed by *Strode et al.* [2008]. During the April and May study period, a number of episodes of enhanced Asian GEM and CO are evident in the model grid box which contained flights 1, 2, 3, 6, and 7. Flights 4 (30 April) and 8 (15 May) were in the adjacent grid box which is not shown. Figure 8 depicts Asian CO and GEM in curtain plots. The flight times are indicated by vertical lines in the time series which are labeled with the flight number. The model simulates a number of strong, well-correlated enhancements of Asian GEM and CO but the timing of the specific enhancements observed in the aircraft on flights 1 (12 April), 2 (18 April), and 6 (8 May) is not well reproduced. The best agreement is seen in flight 6 (8 May) in which a strong plume is present between flights 6 (8 May) and 7 (9 May). For this enhancement, the model predicts a GEM:CO correlation slope (by OLS regression) of 0.0068 ($\text{ng/m}^3/\text{ppb}$) with a significance $p < 1e-4$.

[50] The discrepancy with the model for flight 1 (12 April) could be due to errors in the meteorological fields which affect the horizontal displacement and thus the timing. The lack of an event in the model close to flight 2 (18 April) could also be an artifact of numerical diffusion which can become significant for air parcels stretched into filaments (D. Jacob, personal communication, 2007) which often occurs during LRT.

3.3.3. GEM-CO Relationship in Local Anthropogenic Emissions

[51] Flight 5 (4 May) was conducted to sample the local boundary layer and provide a contrast to the LRT in the free troposphere. The flight was entirely within the boundary layer except for a brief segment at the beginning and end in which the lower free troposphere was sampled to obtain information on the background. During the flight and for at least a day prior, the region was under a surface high pressure system associated with an upper level ridge off the west coast of North America. The lower troposphere was stable with a weak inversion capping the boundary layer. Figure 9 shows scatterplots of ozone, aerosol scattering coefficient, GEM, and water vapor against CO with the points colored by altitude. All of the parameters have different relationships with CO above and below 1500 m, except for GEM.

[52] In the boundary layer, concentrations of CO were enhanced to over 200 ppbv and were strongly correlated with σ_{sp} and water vapor. Ozone had a strong inverse correlation with CO, but GEM was not significantly correlated to CO ($r^2 = 0.054$, $p = 0.21$). Even if the correlation was assumed to be statistically significant, the slope would be 0.00074 $\text{ng/m}^3/\text{ppbv}$, which is an order of magnitude smaller than the Asian anthropogenic emission ratio. The poor correlation of GEM with CO and its lower slope reflect relatively weaker GEM sources in the Seattle-Tacoma area compared to Asian industrial sources. There are no coal-fired power plants in the immediate Seattle-Tacoma region, so the largest GEM sources are likely distilled fuels combustion and waste incineration.

[53] The inverse correlation of ozone and CO indicates there are local sinks for ozone, with chemical loss by reaction with NO emissions being the most plausible mechanism although surface deposition could also contribute to a lesser degree. GEM also does not have a statistically significant relation to ozone ($r^2 = 0.063$, $p = 0.17$), which argues that local anthropogenic pollution and NOx photochemistry (at least in our study region) has a negligible effect on the GEM concentration on the timescale of a few hours.

3.4. GEM Depletion in the Upper Troposphere

[54] The GEM-CO and GEM-ozone relationship observed in several small contiguous pockets of air imply that GEM is, or can be, depleted at the tropopause relative to the mean of the free-troposphere. The episodes occurred in flights 2 (18 April), 5 (4 May), and 6 (8 May), and are listed in Table 5. The font of the correlation slope value indicates its significance as calculated using Kendall's tau which is a more conservative, nonparametric test based on rank order [*Sprent and Smeeton*, 2001]. During these periods, ozone increased and was inversely correlated with GEM and CO. Water vapor was either very low for the

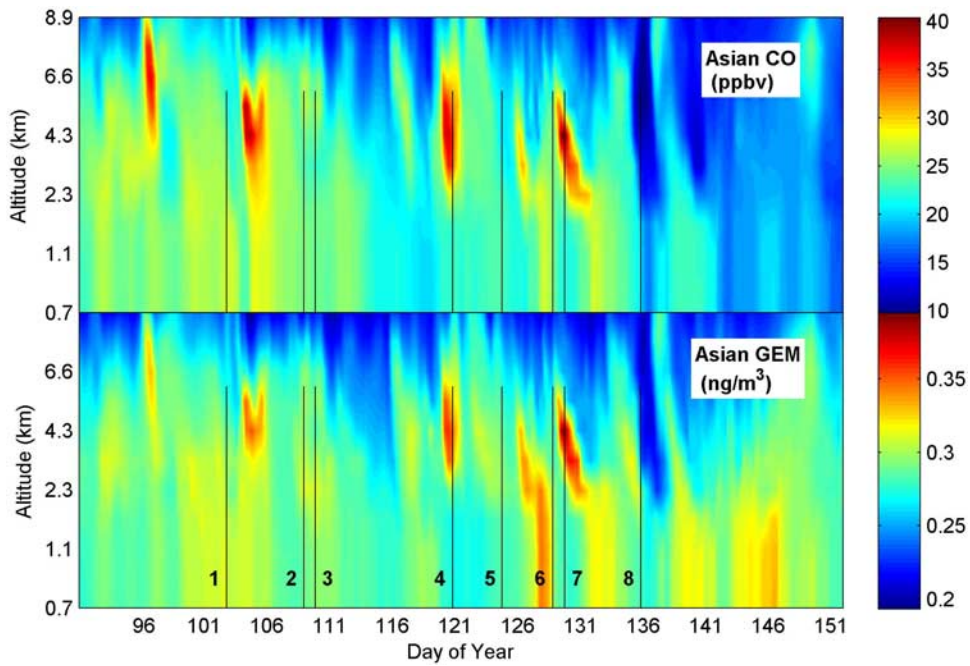


Figure 8. GEOS-Chem modeled tagged Asian CO and GEM in the model grid box centered on 46°N, 125°W. Flight times and maximum altitude are indicated by vertical lines in the time series and the flight number is adjacent to the respective flight.

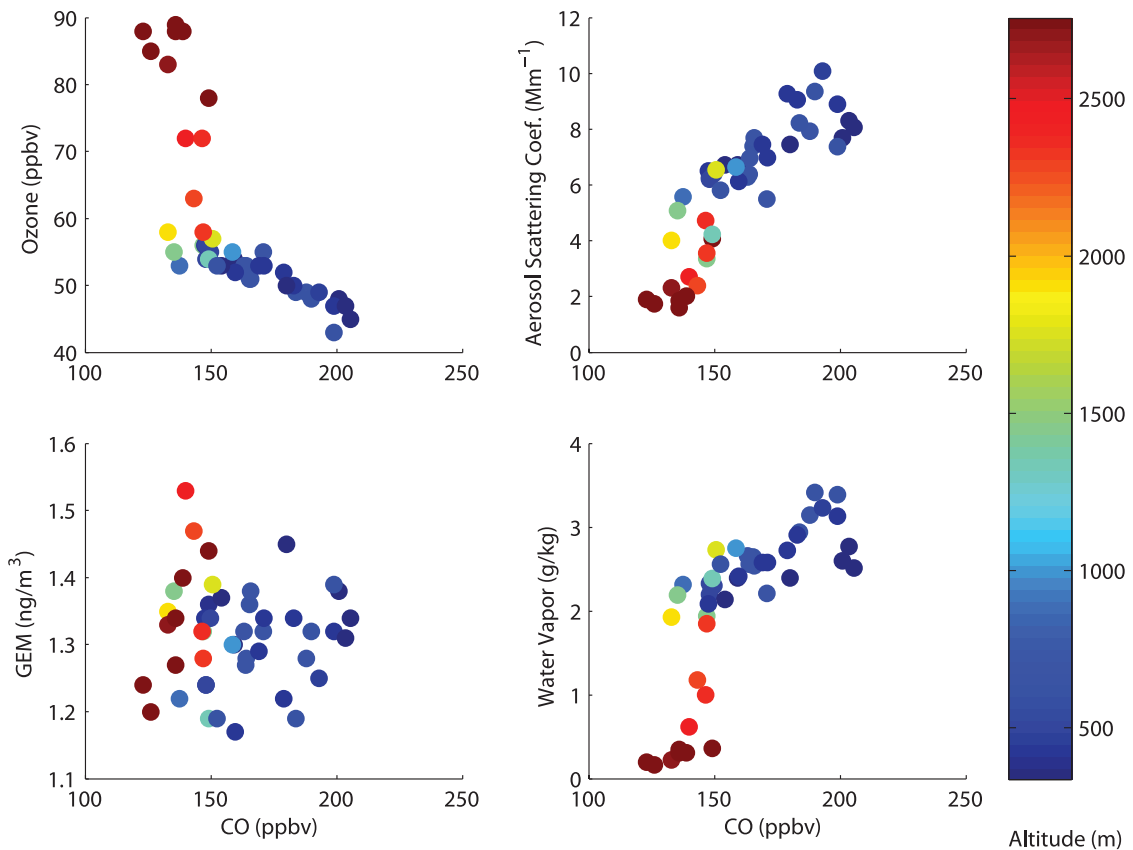


Figure 9. Scatterplots of Flight 5 (4 May) of parameters versus CO, which show the different relationships in the boundary layer versus the free troposphere and the lack of correlation of GEM to CO in local anthropogenic pollution.

Table 5. Summary of Periods of Upper Tropospheric/Stratospheric Influence on Flights 2, 5, and 6^a

Flight	Date	Alt. Range, mb	n	GEM-O ₃		O ₃ -CO		GEM (ng/m ³) at Tropopause ^b	
				RMA Slope	r ²	RMA Slope	r ²	CO (30 ppbv)	O ₃ (200 ppbv)
2	18 Apr	650–500	13	−0.021	0.46	−0.43	0.53	0.57	0
5	4 May	780–730	10	−0.012	0.42	−1.1	0.41	0	0
6	8 May	540–500	11	−0.011	0.66	−1.1	0.90	0.15	0.40

^aAll slopes are significant at $p < 0.05$ and bold font indicates significance at $p < 0.01$.

^bThe concentration of GEM at the tropopause extrapolated from the GEM-CO and GEM-ozone relationship and representative CO and ozone concentrations at the tropopause. See section 3.4.

middle troposphere (<0.2 g/kg, RH $< 10\%$) or the water vapor was inversely correlated with ozone. An example of the GEM and CO relationships to ozone is shown in Figure 10 for flight 6 (8 May). The data from this period are also indicated in Figure 5 with bold x. In contrast to the correlations in the overall data for GEM-ozone ($r = 0.45$) and ozone-CO (0.01), within these periods both the GEM-ozone and ozone-CO correlations are statistically significant and strongly negative, which is consistent with a depletion of GEM with increasing ozone and decreasing CO as is found in the upper troposphere.

[55] The correlation slopes of GEM to ozone and to CO within these periods can be extrapolated to expected tropopause concentrations of both ozone (200 ppbv) and CO (30 ppbv) as reported by *Pan et al.* [2004]. The values from the GEM:CO and GEM:ozone extrapolations for each flight are listed at the right of Table 5. The resulting GEM concentration (mean = 0.19 ng/m³) is much lower than the hemispheric background and total depletion would be reached if the extrapolation was continued into the lower stratosphere. This is not entirely unexpected, and would be consistent with the observations of *Murphy et al.* [2006] which show that in the stratosphere, mercury mass on particles likely exceeds that in the gas phase and observations of *Swartzendruber et al.* [2006] that RGM enhancements in the free troposphere (at MBO) appear to be shifts in speciation (i.e., depletions in GEM) that have an upper tropospheric or stratospheric character. GEM depletion in the lower stratosphere is also consistent with the GEOS-Chem prediction that mercury in the stratosphere is largely in an oxidized state [*Selin et al.*, 2007] and concurrent observations of *Talbot et al.* [2007] who report observations of GEM depletion in the upper troposphere and lower stratosphere.

3.5. Intercomparison With INTEX-B DC-8

[56] During Flight 8 (15 May), an intercomparison was conducted with the DC-8 aircraft from NASA's INTEX-B campaign [*Talbot et al.*, 2008]. The DC-8 and Duchess aircraft flew descending spirals off the southwest coast of Washington state (46.6°N , -124°W) from about 6 km to 1 km within about 30 min. Vertical profiles of GEM, CO, ozone, and water vapor from both aircraft are shown in Figure 11 (all parameters have been averaged to the collection cycles (2.5 min) of the mercury instruments on the respective aircraft). There is good agreement in the CO, ozone, and water vapor between the two platforms in the cluster of data at about 5.5 km and there is excellent agreement for CO throughout the entire profile. There is also generally good agreement below 4 km for CO, water vapor, and ozone. The entire ozone profiles appear to have a slight bias that is close to the uncertainty of our ozone

instrument (about 10%) and would be consistent with a small positive bias in our ozone values as compared to the Trinidad Head ozonesondes (section 3.2). The discrepancy with the two DC-8 ozone points at about 4 and 5 km are likely due to real differences as the aircraft trajectories were about 50 km apart at these altitudes (due to a much larger spiral radius of the DC-8) while the trajectories in the remainder of the profile were within about 15 km. While the uncertainty of the GEM observations ($\sim 10\%$) is greater than for CO, it is not sufficient to explain a mean bias of 30–40%. Since the GEM concentrations observed by each aircraft in this comparison are consistent with the data in the remainder of their respective campaigns and there is agreement in the structure of the GEM profiles and good agreement in the CO, ozone, and water vapor profiles, the most plausible explanation for the GEM discrepancy is a calibration bias and we are continuing to investigate the issue.

4. Conclusions

[57] In this study we measured vertical profiles of gaseous elemental mercury (GEM), CO, ozone, and aerosol scattering coefficient from a small aircraft in the Pacific Northwest of the U.S. We observed several episodes of long-range transport (LRT) of Asian anthropogenic pollution which brought correlated increases in GEM and CO. The mean GEM:CO enhancement ratio (ER) determined by ordinary least squares (OLS) regressions was consistent with previous observations of Asian anthropogenic emis-

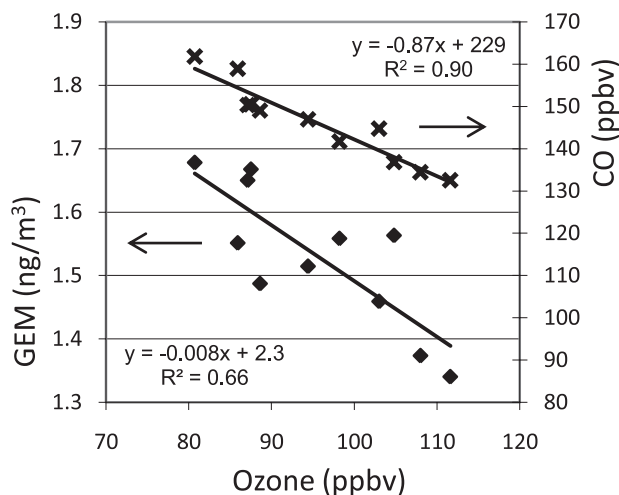


Figure 10. Scatterplot of GEM and CO versus ozone in a pocket of upper tropospheric/stratospheric influence during Flight 6. These points are also indicated in Figure 5.

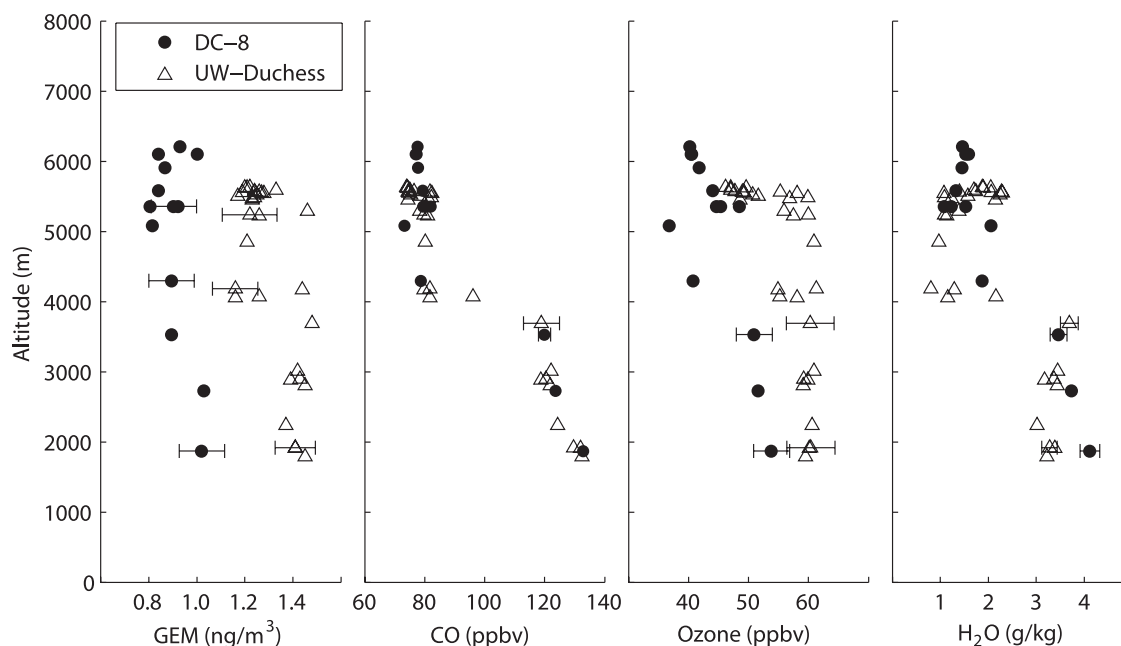


Figure 11. Intercomparison of UW-Duchess and INTEX-B DC-8 observations of GEM, CO, ozone, and water vapor on Flight 8 (15 May) over the southwest coast of Washington state. Error bars which indicate the uncertainty are shown for representative points. See sections 2.2 and 2.3 for descriptions of the uncertainty values.

sions, although the ER determined by reduced major axis regression (RMA) was somewhat higher. The higher ER based on RMA regression implies greater East Asian industrial emission ratios, but the accuracy of this estimate is likely limited by a number of factors including the assumptions of relating an ER to the emission ratio, the validity of the RMA model for this application, limited representativity of three events, or other factors such as seasonality or reemissions. GEM and CO in the Seattle-Tacoma boundary layer was not significantly correlated and the ER was an order of magnitude smaller than in Asian industrial LRT, which reflects weaker sources of GEM in local anthropogenic emissions. We also observed a bimodal distribution of ozone which roughly corresponded to a separation of free-tropospheric and boundary layer influence. The higher ozone mode also contained significantly greater GEM, but CO and aerosol scattering coefficient were not significantly different. Several small pockets of air with upper free tropospheric characteristics were observed. This air contained enhanced ozone which was inversely correlated to CO and GEM and, when extrapolated to higher altitudes, implies that GEM can be largely depleted in the upper troposphere.

[58] **Acknowledgments.** Funding for this research was provided by an EPA STAR grant (R-82979701). It has not been subjected to any EPA review and does not necessarily reflect the view of the agency. This research would not have been possible without the assistance of Northway Aviation and their pilots. P. Swartzendruber also wishes to acknowledge helpful discussions with Chris Holmes, Daniel Jacob, Eric Prestbo, and the helpful comments of the anonymous reviewers.

References

Ayers, G. P. (2001), Comment on regression analysis of air quality data, *Atmos. Environ.*, *35*(13), 2423–2425, doi:10.1016/S1352-2310(00)00527-6.

- Banic, C. M., S. T. Beauchamp, R. J. Tordon, W. H. Schroeder, A. Steffen, K. A. Anlauf, and H. K. T. Wong (2003), Vertical distribution of gaseous elemental mercury in Canada, *J. Geophys. Res.*, *108*(D9), 4264, doi:10.1029/2002JD002116.
- Bertschi, I. B., and D. A. Jaffe (2005), Long-range transport of ozone, carbon monoxide and aerosols to the NE Pacific troposphere during the summer of 2003: Observations of smoke plumes from Asian Boreal fires, *J. Geophys. Res.*, *110*, D05303, doi:10.1029/2004JD005135.
- Bertschi, I. B., D. A. Jaffe, L. Jaegle, H. U. Price, and J. B. Dennison (2004), PHOBEA/ITCT 2002 airborne observations of trans-Pacific transport of ozone, CO, VOCs and aerosols to the northeast Pacific: Impacts of Asian anthropogenic and Siberian Boreal fire emissions, *J. Geophys. Res.*, *109*, D23S12, doi:10.1029/2003JD004328.
- Carmichael, G. R., et al. (2003), Evaluating regional emission estimates using the TRACE-P observations, *J. Geophys. Res.*, *108*(D21), 8810, doi:10.1029/2002JD003116.
- Chand, D., P. Guyon, P. Artaxo, O. Schmid, G. P. Frank, L. V. Rizzo, O. L. Mayol-Bracero, L. V. Gatti, and M. O. Andreae (2006), Optical and physical properties of aerosols in the boundary layer and free troposphere over the Amazon Basin during the biomass burning season, *Atmos. Chem. Phys.*, *6*, 2911–2925.
- Cooper, O. R., et al. (2004), A case study of transpacific warm conveyor belt transport: Influence of merging airstreams on trace gas import to North America, *J. Geophys. Res.*, *109*, D23S08, doi:10.1029/2003JD003624.
- Draper, N. R., and H. Smith (1998), *Applied Regression Analysis*, 3rd ed., John Wiley, New York.
- Draxler, R. R., and G. D. Rolph (2003), HYSPLIT (HYbrid Single-Particle Lagrangian Integrated Trajectory) model access via NOAA ARL READY website, NOAA Air Resour. Lab., Silver Spring, Md. (Available at <http://www.arl.noaa.gov/ready/hysplit4.html>)
- Ebinghaus, R., and F. Slemr (2000), Aircraft measurements of atmospheric mercury over southern and eastern Germany, *Atmos. Environ.*, *34*, 895–903, doi:10.1016/S1352-2310(99)00347-7.
- Ebinghaus, R., F. Slemr, C. A. M. Brenninkmeijer, P. van Velthoven, A. Zahn, M. Hermann, D. A. O'Sullivan, and D. E. Oram (2007), Emissions of gaseous mercury from biomass burning in South America in 2005 observed during CARIBIC flights (2007), *Geophys. Res. Lett.*, *34*, L08813, doi:10.1029/2006GL028866.
- Friedli, H. R., L. F. Radke, R. Prescott, P. Li, J.-H. Woo, and G. R. Carmichael (2004), Mercury in the atmosphere around Japan, Korea, and China as observed during the 2001 ACE-Asia field campaign: Measurements, distributions, sources, and implications, *J. Geophys. Res.*, *109*, D19S25, doi:10.1029/2003JD004244.

- Holzer, M., and T. M. Hall (2007), Low-level transpacific transport, *J. Geophys. Res.*, *112*, D09103, doi:10.1029/2006JD007828.
- Jaffe, D., E. Prestbo, P. Swartzendruber, P. Weiss-Penzias, S. Kato, A. Takami, S. Hatakeyama, and Y. Kajii (2005), Export of atmospheric mercury from Asia, *Atmos. Environ.*, *39*, 3029–3038, doi:10.1016/j.atmosenv.2005.01.030.
- Kotchenruther, R. A., D. A. Jaffe, H. J. Beine, T. Anderson, J. W. Bottenheim, J. M. Harris, D. Blake, and R. Schmitt (2001), Observations of ozone and related species in the Northeast Pacific during the PHOBEA campaigns: 2. Airborne observations, *J. Geophys. Res.*, *106*, 7463–7483, doi:10.1029/2000JD900425.
- Landis, M. S., M. Lynam, and R. K. Stevens (2005), The monitoring and modeling of mercury species in support of local, regional, and global modeling, in *Dynamics of Mercury Pollution on Regional and Global Scales*, edited by N. Pirrone and K. R. Mahaffy, pp. 123–151, Kluwer Acad., New York.
- Lin, C. J., P. Pongprueksa, S. E. Lindberg, S. O. Pehkonen, D. Byun, and C. Jang (2006), Scientific uncertainties in atmospheric mercury models: I. Model science evaluation, *Atmos. Environ.*, *40*, 2911–2928, doi:10.1016/j.atmosenv.2006.01.009.
- Lohman, K., C. Seigneur, E. Edgerton, and J. Jansen (2006), Modeling mercury in power plant plumes, *Environ. Sci. Technol.*, *40*(12), 3848–3854, doi:10.1021/es051556v.
- Mitchell, A. C. G., and M. W. Zemansky (1971), *Resonance and Radiation and Excited Atoms*, Cambridge Univ. Press, New York.
- Murphy, D. M., P. K. Hudson, D. S. Thomson, P. J. Sheridan, and J. C. Wilson (2006), Observations of mercury containing aerosols, *Environ. Sci. Technol.*, *40*, 3163–3167, doi:10.1021/es052385x.
- Pacyna, E. G., and J. M. Pacyna (2002), Global emission of mercury from anthropogenic sources in 1995, *Water Air Soil Pollut.*, *137*, 149–165, doi:10.1023/A:1015502430561.
- Pan, L. L., W. J. Randel, B. L. Gary, M. J. Mahoney, and E. J. Hintsa (2004), Definitions and sharpness of the extratropical tropopause: A trace gas perspective, *J. Geophys. Res.*, *109*, D23103, doi:10.1029/2004JD004982.
- Parrish, D. D., Y. Kondo, O. R. Cooper, C. A. Brock, D. A. Jaffe, M. Trainer, T. Ogawa, G. Hübler, and F. C. Fehsenfeld (2004), Intercontinental transport and chemical transformation 2002 (ITCT 2K2) and Pacific exploration of Asian continental emission (PEACE) experiments: An overview of the 2002 winter and spring intensives, *J. Geophys. Res.*, *109*, D23S01, doi:10.1029/2004JD004980.
- Price, H. U., D. A. Jaffe, P. V. Doskey, I. McKendry, and T. L. Anderson (2003), Vertical profiles of O₃, aerosols, CO and NMHCs in the Northeast Pacific during the Trace-P and ACE-Asia experiments, *J. Geophys. Res.*, *108*(D20), 8799, doi:10.1029/2002JD002930.
- Price, H. U., D. A. Jaffe, O. R. Cooper, and P. V. Doskey (2004), Photochemistry, ozone production, and dilution during long-range transport episodes from Eurasia to the northwest United States, *J. Geophys. Res.*, *109*, D23S13, doi:10.1029/2003JD004400.
- Schroeder, W. H., and J. Munthe (1998), Atmospheric Mercury: An overview, *Atmos. Environ.*, *32*(5), 809–822, doi:10.1016/S1352-2310(97)00293-8.
- Selin, N. E., D. Jacob, R. Park, R. M. Yantosca, S. Strode, L. Jaeglé, C. Holmes, and D. A. Jaffe (2007), Chemical cycling and deposition of atmospheric mercury: Global constraints from observations, *J. Geophys. Res.*, *112*, D02308, doi:10.1029/2006JD007450.
- Slemr, F., G. Schuster, and W. Seiler (1985), Distribution, speciation, and budget of atmospheric mercury, *J. Atmos. Chem.*, *3*, 407–434, doi:10.1007/BF00053870.
- Slemr, F., R. Ebinghaus, P. G. Simmonds, and S. G. Jennings (2006), European emissions of mercury derived from long-term observations at Mace Head, on the western Irish coast, *Atmos. Environ.*, *40*, 6966–6974, doi:10.1016/j.atmosenv.2006.06.013.
- Snow, J. A., J. B. Dennison, D. A. Jaffe, H. U. Price, J. K. Vaughan, and B. Lamb (2003), Aircraft and surface observations in Puget Sound and a comparison to a regional model, *Atmos. Environ.*, *37*, 4019–4032, doi:10.1016/S1352-2310(03)00429-1.
- Sprent, P., and N. C. Smeeton (2001), *Applied Nonparametric Statistical Methods*, Chapman and Hall, London.
- Strode, S., L. Jaeglé, D. A. Jaffe, P. C. Swartzendruber, N. E. Selin, C. Holmes, and R. Yantosca (2008), Trans-Pacific transport of Mercury, *J. Geophys. Res.*, doi:10.1029/2007JD009428, in press.
- Swartzendruber, P. C., D. A. Jaffe, E. M. Prestbo, P. Weiss-Penzias, N. E. Selin, R. Park, D. J. Jacob, S. Strode, and L. Jaeglé (2006), Observations of reactive gaseous mercury in the free troposphere at the Mount Bachelor Observatory, *J. Geophys. Res.*, *111*, D24301, doi:10.1029/2006JD007415.
- Talbot, R., H. Mao, E. Scheuer, J. Dibb, and M. Avery (2007), Total depletion of Hg⁰ in the upper troposphere–lower stratosphere, *Geophys. Res. Lett.*, *34*, L23804, doi:10.1029/2007GL031366.
- Talbot, R., et al. (2008), Factors influencing the large-scale distribution of Hg⁰ in the Mexico City area and over the North Pacific, *Atmos. Chem. Phys.*, *8*, 2103–2114.
- Tekran (2006), Comparison of gaseous mercury vapor calibrations with NIST traceable liquid standards, technical memorandum, Tekran Instruments Corp., Knoxville, Tenn.
- Temme, C., J. W. Einax, R. Ebinghaus, and W. H. Schroeder (2003), Measurements of atmospheric mercury species at a coastal site in the Antarctic and over the South Atlantic Ocean during polar sunrise, *Environ. Sci. Technol.*, *37*, 22–31.
- Weiss-Penzias, P., D. A. Jaffe, A. McClintick, E. M. Prestbo, and M. S. Landis (2003), Gaseous elemental mercury in the marine boundary layer: Evidence for rapid removal in anthropogenic pollution, *Environ. Sci. Technol.*, *37*, 3755–3763, doi:10.1021/es0341081.
- Weiss-Penzias, P., D. A. Jaffe, P. C. Swartzendruber, J. B. Dennison, D. Chand, and E. M. Prestbo (2006), Observations of Asian air pollution in the free troposphere at Mt. Bachelor Observatory during the spring of 2004, *J. Geophys. Res.*, *111*, D10304, doi:10.1029/2005JD006522.
- Weiss-Penzias, P., D. A. Jaffe, P. C. Swartzendruber, W. Hafner, D. Chand, and E. M. Prestbo (2007), Quantifying Asian and biomass burning sources of mercury using the Hg/CO ratio in pollution plumes observed at the Mount Bachelor observatory, *Atmos. Environ.*, *41*(21), 4366–4379, doi:10.1016/j.atmosenv.2007.01.058.
- Wilcox, R. R. (2005), *Introduction to Robust Estimation and Hypothesis Testing*, 2nd ed., Elsevier, Burlington, Mass.

D. Chand, L. Jaeglé, D. A. Jaffe, D. Reidmiller, S. Strode, and P. C. Swartzendruber, Department of Atmospheric Sciences, University of Washington, Seattle, WA 98195-1640, USA. (pswartz@u.washington.edu)
L. Gratz and J. Keeler, Air Quality Laboratory, University of Michigan, Ann Arbor, MI 48109, USA.

J. Smith, Interdisciplinary Arts and Sciences, University of Washington-Bothell, Bothell, WA 98011-8246, USA.

R. Talbot, Institute for the Study of Earth, Oceans, and Space, University of New Hampshire, Durham, NH 03824, USA.